Supplementary Information (SI) for Soft Matter.

Supplementary Information to Development of coarse-grained molecular dynamics model for poly(dimethyl-*co*-diphenyl)siloxane

Weikang Xian,[a] Amitesh Maiti,[b] Andrew P. Saab [b] and Ying Li*[a]

a. Department of Mechanical Engineering, University of Wisconsin-Madison, Madison, Wisconsin 53706-1572, USA. E-mail: yli2562@wisc.edu;

b. Lawrence Livermore National Laboratory, Livermore, California 94550 USA

AAMD referential structural distributions. All structural distributions for bond, angle and dihedral interactions are shown in from Figs. S1 to S3 respectively. Blue lines are the average distributions over all systems with different ϕ. Green areas are the variations. We assumed that the variations are insignificant such that we used the average distributions to optimize the CG potentials. In addition, the optimized CG bonded potentials remain unchanged for all simulations.

Coarse-grained mapping scheme. In the main text, the first mapping scheme coarse-grained (CG) beads are selected as the dimethyl and diphenyl silicon atoms. Here, we present the second mapping scheme for pure polydiphenylsiloxane (PDPS). The geometrical centres of the diphenyl side group are chosen as the locations of the other types of CG beads. A PDPS molecule is shown in Fig. S4, where (a) is the AA representation of the molecule. Fig. S4 (b) and (c) are the first and the second mapping scheme, respectively. Results of structural distributions for the alternative mapping scheme are shown in Figs. S5 to S8. Results of structural distributions for the first mapping scheme, are shown in Fig. S9. For comparison, conformation of individual chains is shown in Fig. S10, quantified by the distributions of the mean-squared end-to-end distance, mean-squared radius of gyration, and eigenvalues of the gyration tensor. The first mapping scheme is preferable because it is more computationally efficient but also capture the structural characteristics of the AA ground truth.

Validation for systems with synthetic pair potential. As mentioned in the main text, we did not optimize pair potentials of systems with ϕ=0.05, 0.1, and 0.15. We synthesized them instead according to the lever rule defined in the main text. Bond, angle, and dihedral distributions from the CG simulation with the synthetic potentials were compared with the target AA ground truth.

Results are shown in from Figs. S11 to S13. It is worth noting that the dashed lines are the target distributions based on which the CG bonded potentials were trained. Solid lines are the AA distributions for with ϕ=0.05, 0.1, and 0.15 but they were not included in the target AA ground truth. Symbols are distribution from the CG simulation with the synthetic potentials.

Other structural characterization of the CG systems. In Fig. S14, overall structural factor for AA referential systems and the CG counterparts are compared. It is shown that the CG model captures very well the packing characteristics of the AA systems as locations of the peak match. In Fig. S15, mean-squared end-to-end distance, mean-squared radius of gyration are shown for all systems with N=100. In Fig. S16, values of characteristic ratio for all systems are evaluated by the normalized mean-square internal distance. The results of the structural characteristics for the entangled systems (i.e., Fig. 10 in the main text) are plotted as functions of ϕ, as shown in Fig. S17, for readers in interest.

List of labels for all bonded and non-bonded interactions is as in Table S1.

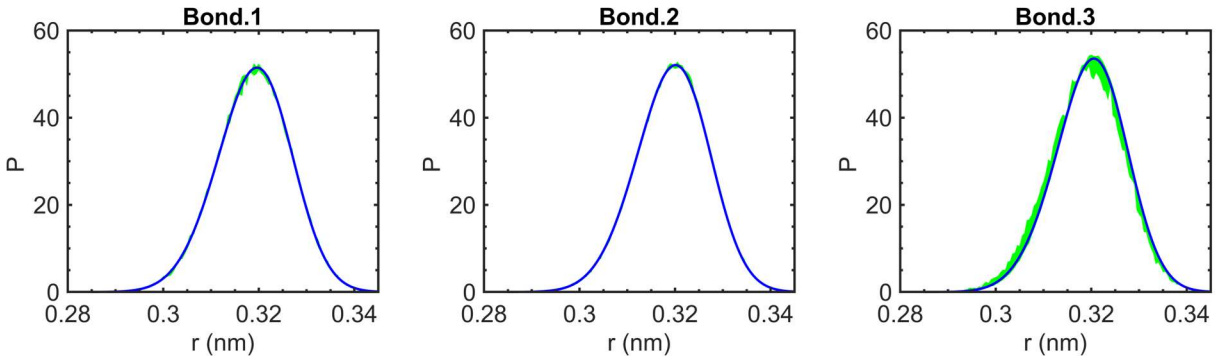

Figure S1. Bond distributions from the AAMD simulations. Blue lines are the average over all systems with different ϕ. The green shade areas represent the variation of the distributions.

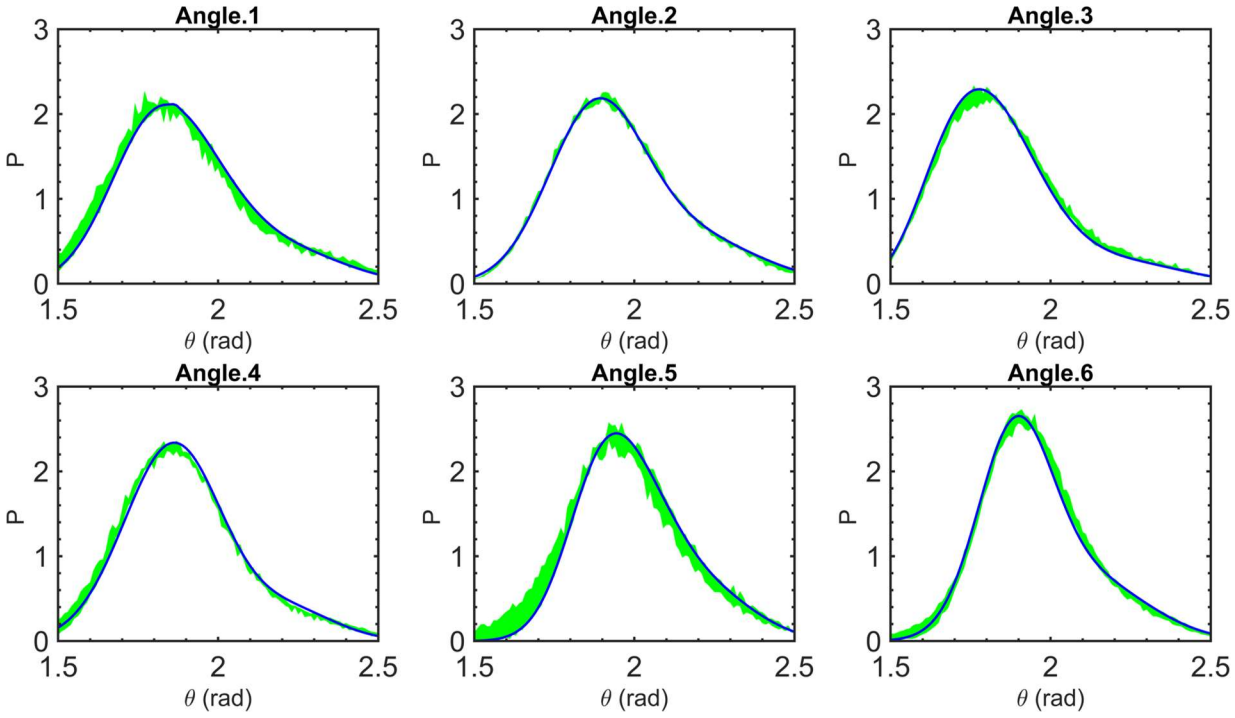

Figure S2. Angle distributions from the AAMD simulations. Blue lines are the average over all systems with different ϕ. The green shade areas represent the variation of the distributions.

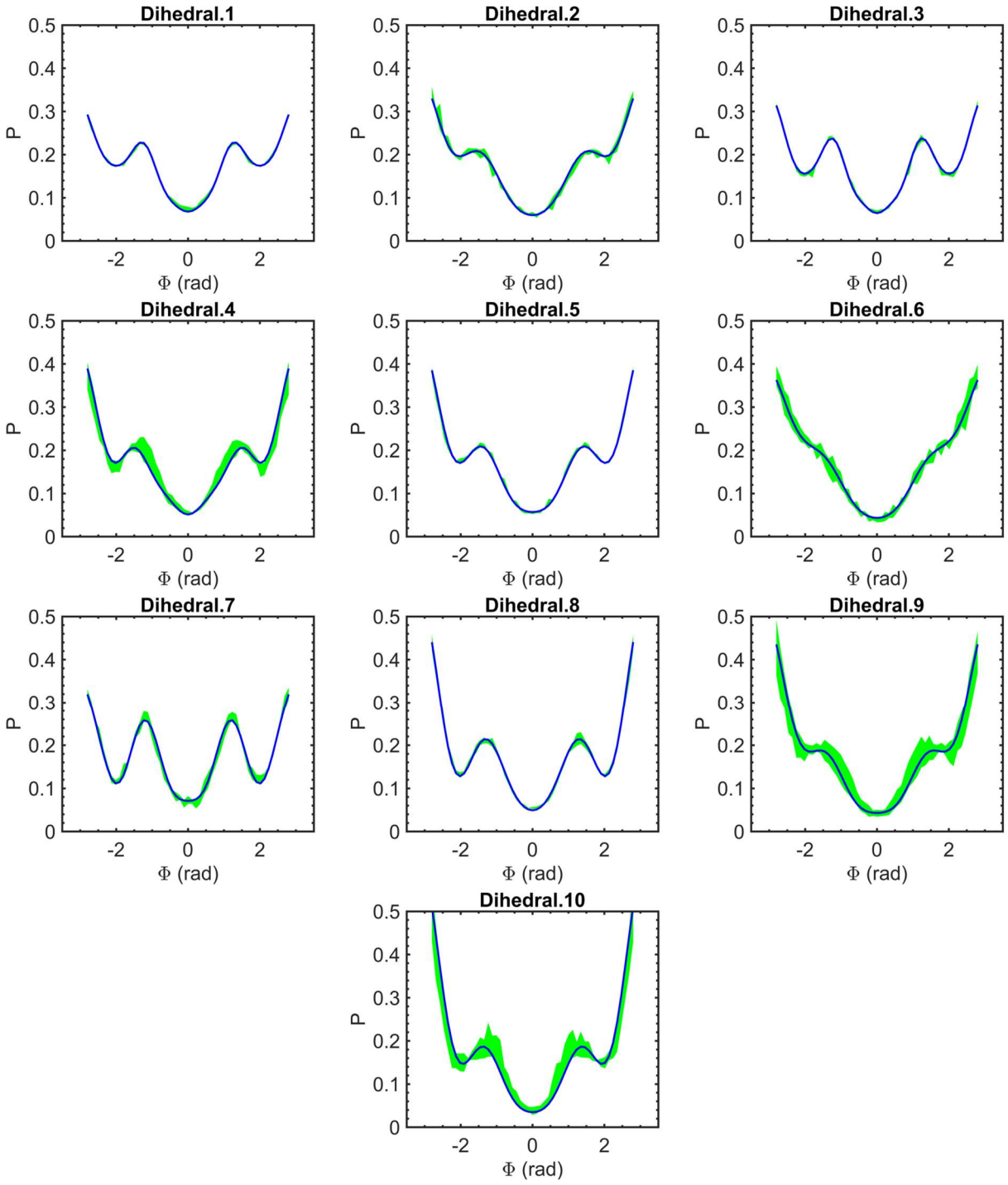

Figure S3. Dihedral distributions from the AAMD simulations. Blue lines are the average over all systems with different ϕ. The green shade areas represent the variation of the distributions.

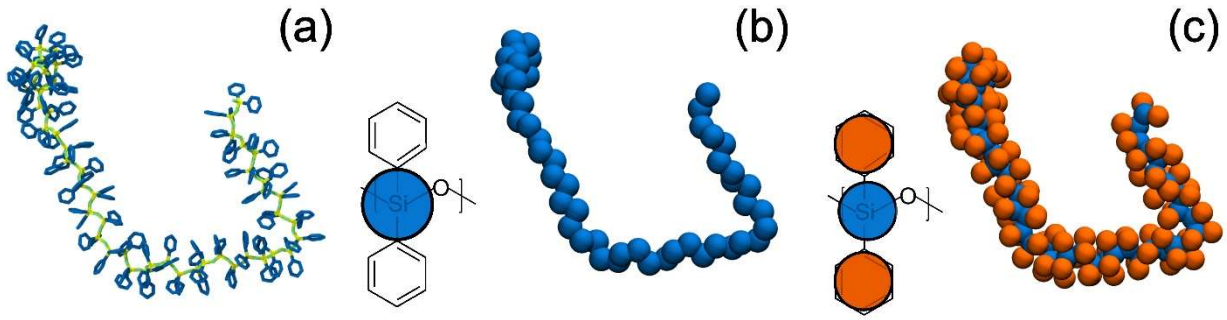

Figure S4. Alternative mapping scheme. (a) is a PDPS molecule in AA representation. (b) and (c) are the CG representations according to the first and the alternative mapping schemes, respectively. In the alternative mapping scheme, geometric centres of the phenyl groups are defined as the side beads.

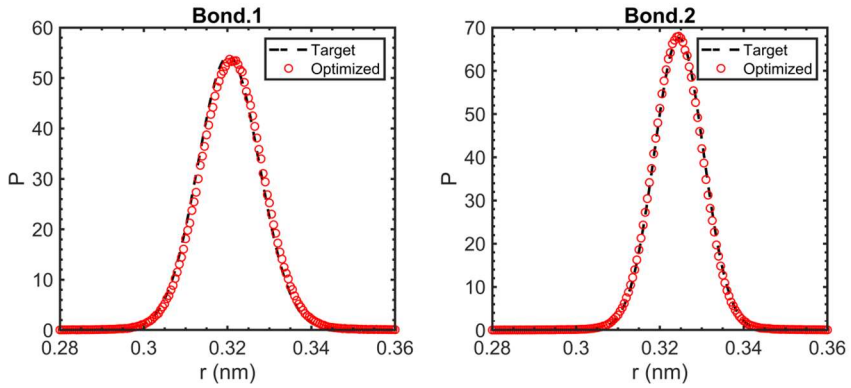

Figure S5. Bond distributions for the alternative mapping scheme.

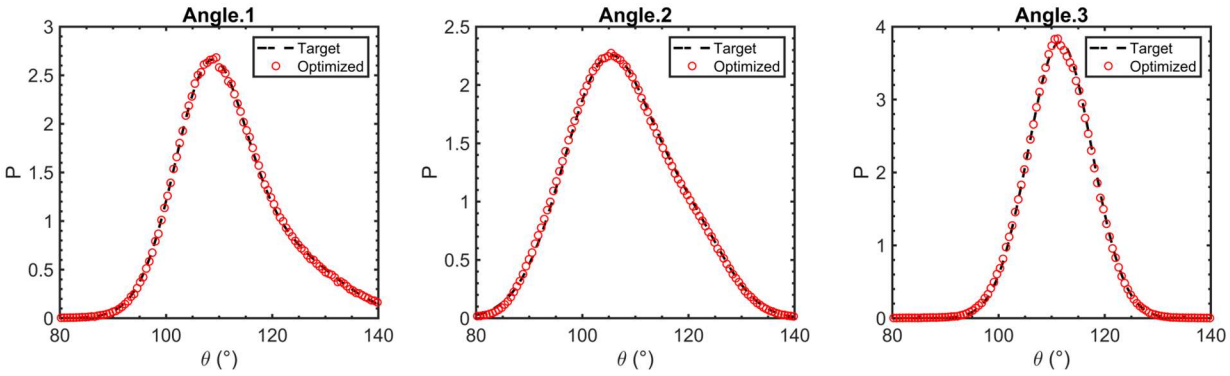

Figure S6. Angle distributions for the alternative mapping scheme.

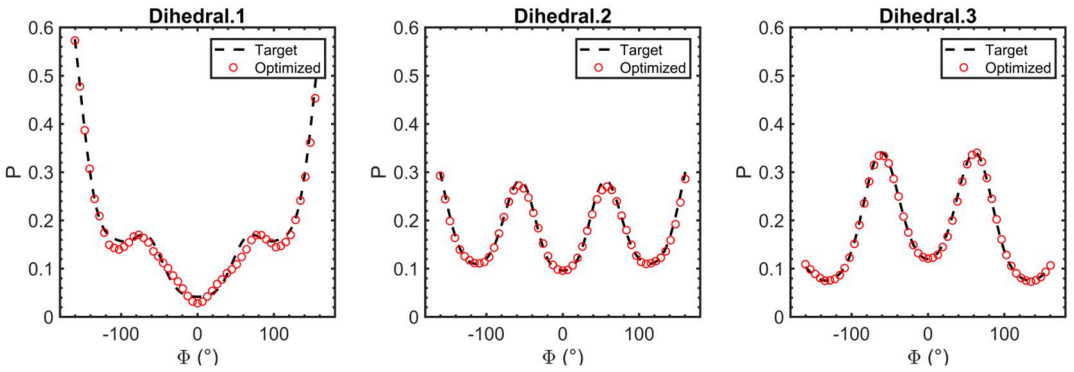

Figure S7. Dihedral distributions for the alternative mapping scheme.

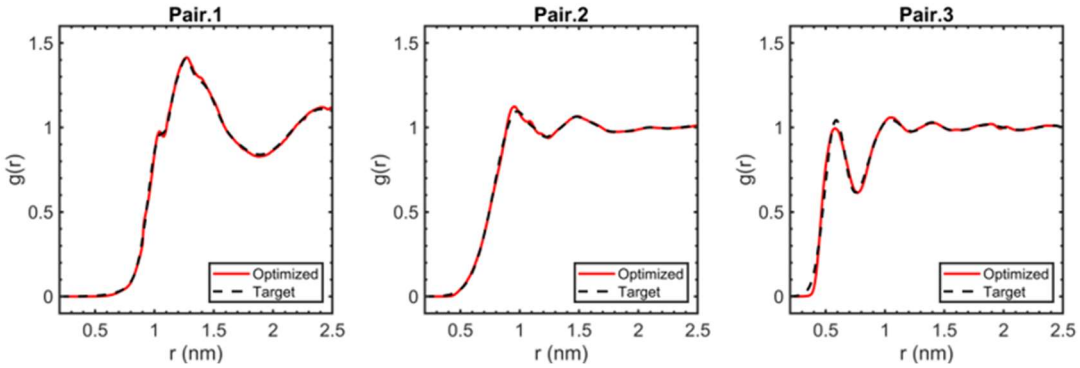

Figure S8. Pair distributions (RDFs) for the alternative mapping scheme.

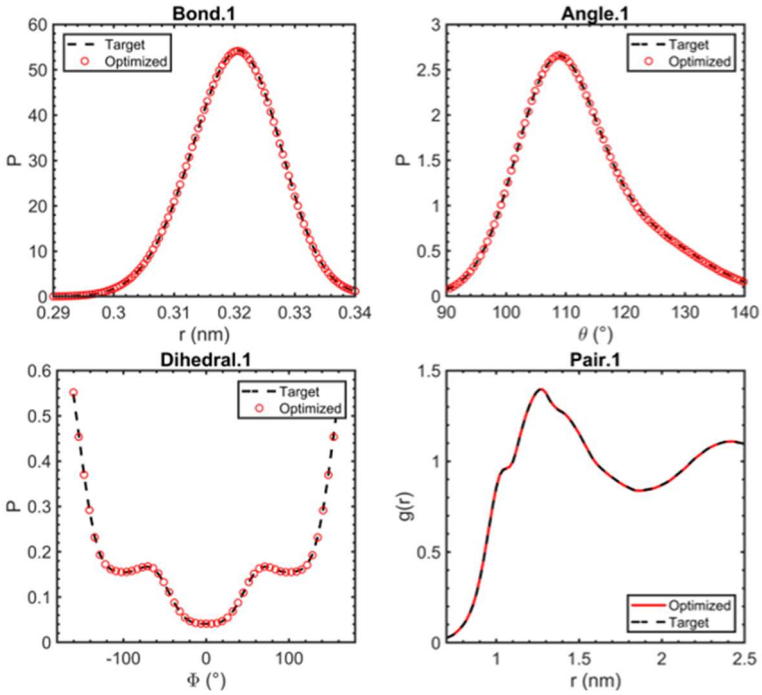

Figure S9. Structural distributions for the first mapping scheme applied to pure polydiphenylsiloxane (PDPS).

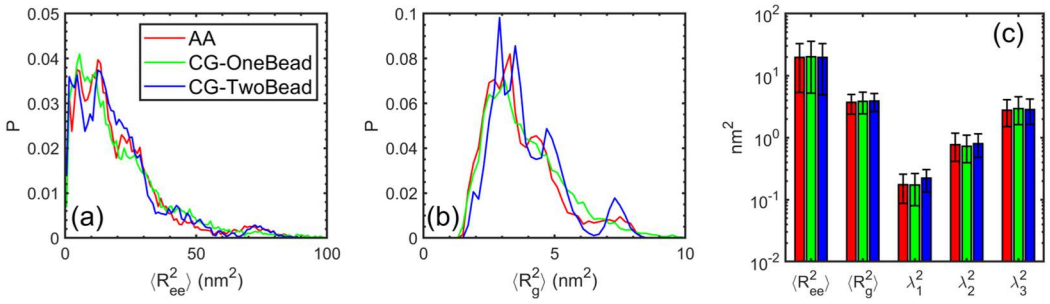

Figure S10. Conformation of individual chains comparing results from both mapping schemes with AA ground truth for PDPS. (a) probability distribution of mean-squared end-to-end distance, $\langle R_{ee}^2 \rangle$. (b) probability distribution of mean-squared radius of gyration, $\langle R_g^2 \rangle$. (c) a direct comparison of $\langle R_{ee}^2 \rangle$, $\langle R_g^2 \rangle$, and eigenvalues of the gyration tensor.

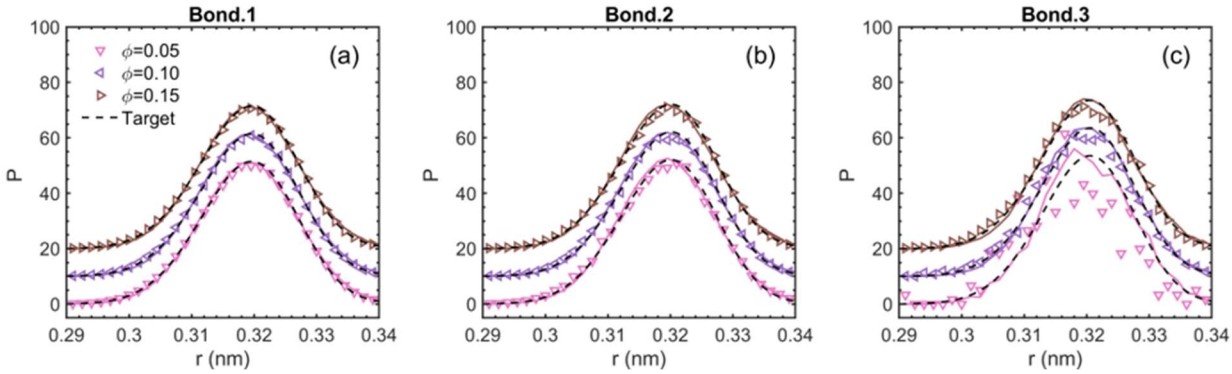

Figure S11. Validation of the bond distributions for the systems with synthetic pair potentials.

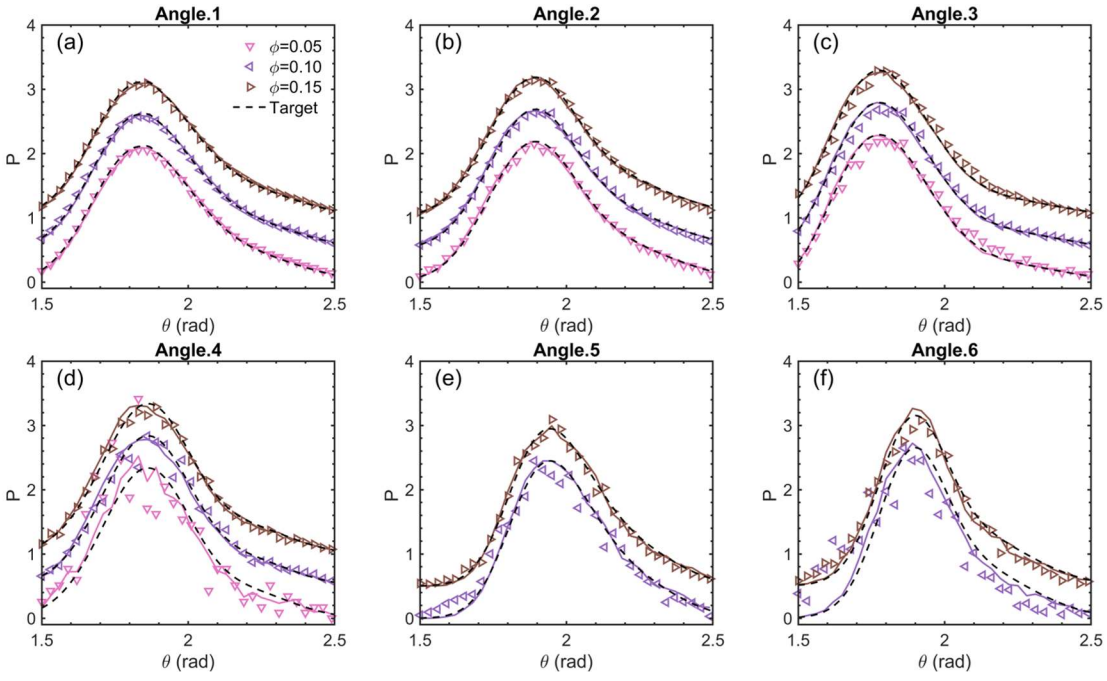

Figure S12. Validation of the angle distributions for the systems with synthetic pair potentials.

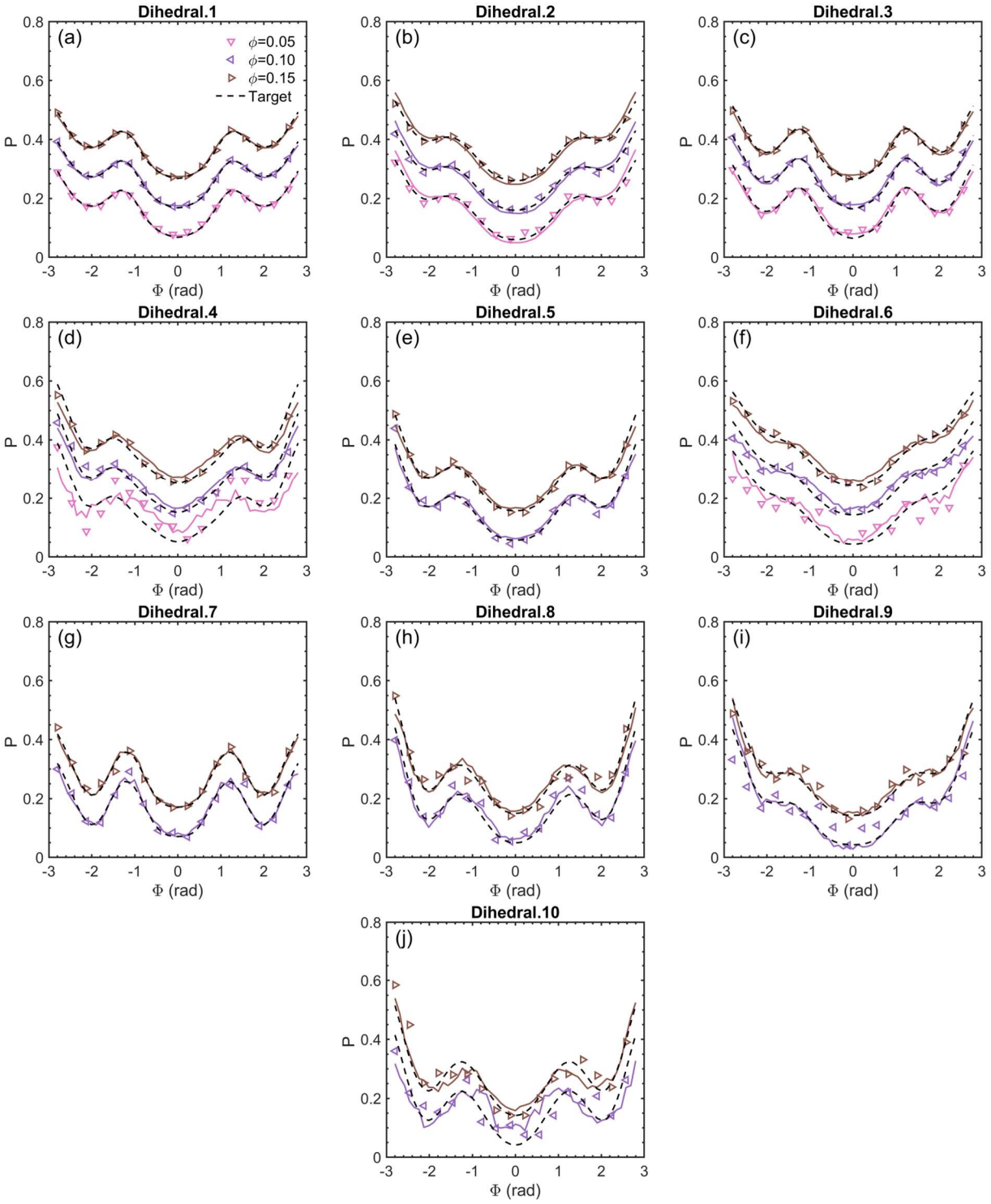

Figure S13. Validation of the dihedral distributions for the systems with synthetic pair potentials.

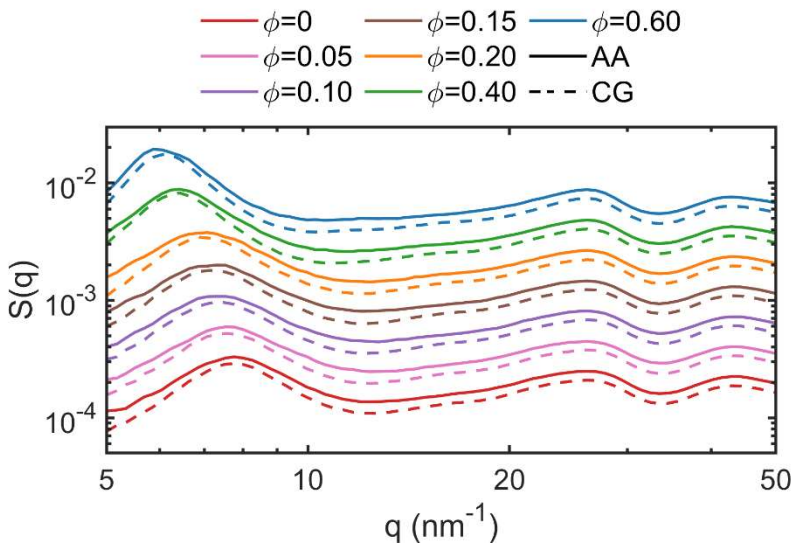

Figure S14. Overall structure factor for AA referential (solid lines) and CG results (dashed lines). The CG results peaks match with the AA results accurately.

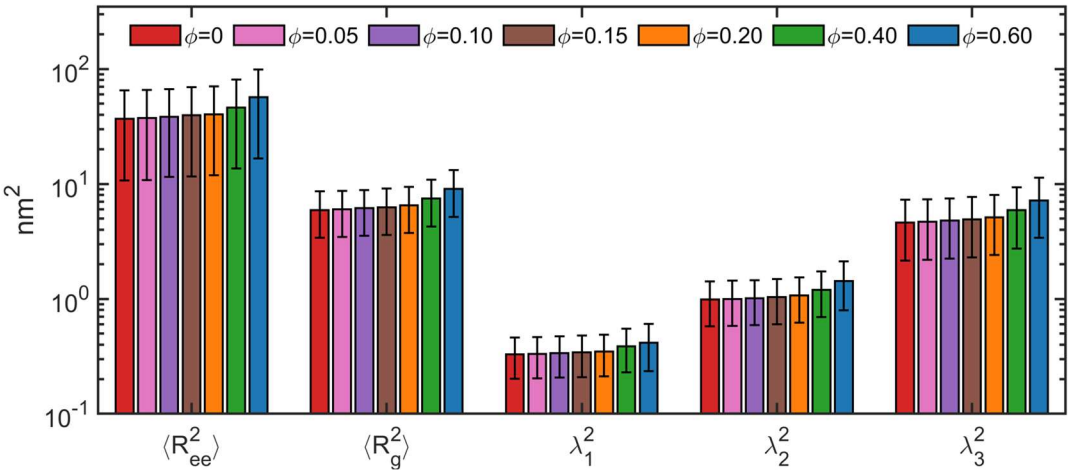

Figure S15. Conformation of individual chains comparing results from both mapping schemes with AA ground truth for all systems with N=100, including mean-squared end-to-end distance, mean-squared radius of gyration, and eigenvalues of the gyration tensor.

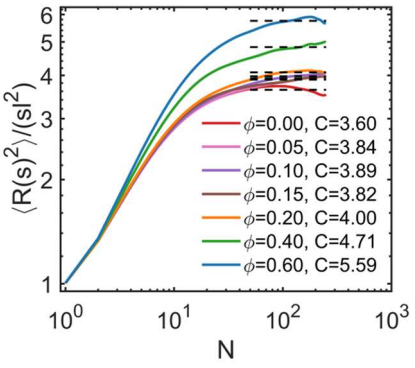

Figure S16. Characteristic ratio for all systems, estimated by the normalized mean-squared internal end-to-end distance.

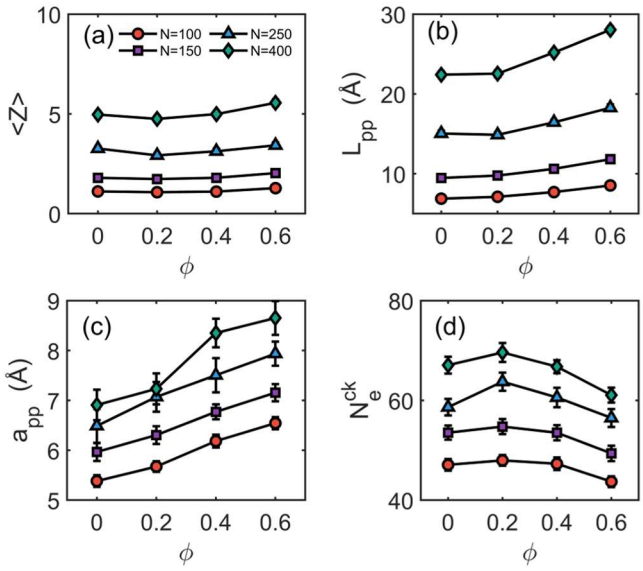

Figure S17. Results of structural characteristics for the entangled system as functions of ϕ.

Table S1. Detailed list of labels for bonded and non-bonded interactions. CGB1 (red) and CGB2 (blue) represent dimethyl and diphenyl CG beads respectively. Hyphen and triple hyphen stand for bonded and non-bonded interactions.

Bond type		
(1) CGB1-CGB1	(2) CGB1-CGB2	(3) CGB2-CGB2
Angle type		
(1) CGB1-CGB1-CGB1	(2) CGB1-CGB1-CGB2	(3) CGB1-CGB2-CGB1
(4) CGB1-CGB2-CGB2	(5) CGB2-CGB1-CGB2	(6) CGB2-CGB2-CGB2
Dihedral type		
(1) CGB1-CGB1-CGB1-CGB1	(2) CGB1-CGB1-CGB1-CGB2	(3) CGB1-CGB1-CGB2-CGB1
(4) CGB1-CGB1-CGB2-CGB2	(5) CGB1-CGB2-CGB1-CGB2	(6) CGB2-CGB1-CGB1-CGB2
(7) CGB1-CGB2-CGB2-CGB1	(8) CGB1-CGB2-CGB2-CGB2	(9) CGB2-CGB1-CGB2-CGB2
	(10) CGB2-CGB2-CGB2-CGB2	
Pair type		
(1) CGB1---CGB1	(2) CGB1---CGB2	(3) CGB2---CGB2